



HAL
open science

Analysis of morphological variations of flax fibre bundles by Fraunhofer diffraction

Komlavi Gogoli, Florian Gehring, Christophe Poilâne, Magali Morales

► To cite this version:

Komlavi Gogoli, Florian Gehring, Christophe Poilâne, Magali Morales. Analysis of morphological variations of flax fibre bundles by Fraunhofer diffraction. *Industrial Crops and Products*, 2021, 171, pp.113856. 10.1016/j.indcrop.2021.113856 . hal-03348176

HAL Id: hal-03348176

<https://hal.science/hal-03348176v1>

Submitted on 2 Aug 2023

HAL is a multi-disciplinary open access archive for the deposit and dissemination of scientific research documents, whether they are published or not. The documents may come from teaching and research institutions in France or abroad, or from public or private research centers.

L'archive ouverte pluridisciplinaire **HAL**, est destinée au dépôt et à la diffusion de documents scientifiques de niveau recherche, publiés ou non, émanant des établissements d'enseignement et de recherche français ou étrangers, des laboratoires publics ou privés.



Distributed under a Creative Commons Attribution - NonCommercial 4.0 International License

1 **Analysis of morphological variations of flax fibre bundles by Fraunhofer** 2 **diffraction**

3 **Komlavi Gogoli^{1,*}, Florian Gehring¹, Christophe Poilâne¹, Magali Morales¹**

4 1. Normandie Univ, ENSICAEN, UNICAEN, CEA, CNRS, CIMAP, 14050, Caen, France

5 **Abstract**

6 The increasing use of plant fibres in industrial applications requires a better understanding of
7 their morphologies. Experimental observations have shown that these fibres are characterized
8 by a complex geometry which could affect their mechanical behaviour. Indeed, it is well
9 known that the size and shape of plant fibres cross-section vary from bundle to bundle and
10 along their length. In this study, the technique of Fraunhofer diffraction was used to
11 characterize this morphological heterogeneity of flax fibre bundles. The analysis of the results
12 showed a large scattering of the cross-section area (CSA). Lengthwise morphological
13 variations of the bundles were examined and reveal that the CSA varies by a factor of 3.4 over
14 a length of 75 mm. It also appears that the cross-section shape of flax fibre bundle can be
15 better approximated by an elliptical model than by a circular model. The ratio between the
16 maximum and minimum cross-section shape factor was found to be approximately 2 over a
17 length of 75 mm. Moreover, the occurrence of cross-section rotations has been shown in case
18 of fibre bundles, i.e., the orientation of the major-axis of the ellipse corresponding to the
19 cross-section may be different from one point to another, causing sometimes visible twists
20 along the bundle. These different results allowed us to build a numerical 3D volume
21 considering the evolution of flax fibre bundles outer contour.

22 **Keywords:** flax fibre bundle; Fraunhofer diffraction; cross-section area; shape factor; variability; 3D
23 reconstruction

* Corresponding author at: Normandie Univ, ENSICAEN, UNICAEN, CEA, CNRS, CIMAP, 14000, Caen, France;
E-mail address: alphonse.gogoli@unicaen.fr

24 **1. Introduction**

25 As a response to ecological challenges, there is an increasing use of plant fibres in industry,
26 particularly in the manufacture of composite materials (Dicker et al., 2014; Joshi et al., 2004).
27 As they are biodegradable, renewable and naturally abundant, these plant resources offer real
28 alternatives to petrochemical fibres (Goda and Cao, 2007). Used in particular as
29 reinforcements in organic matrix composite materials, plant fibres such as flax, sisal or hemp
30 have remarkable specific mechanical properties making them very competitive with man-
31 made materials such as glass (Bledzki and Gassan, 1999; Wambua et al., 2003; Yan et al.,
32 2014). In the fight against global warming, these plant fibres are therefore good candidates to
33 replace petrochemicals fibers as their increasing use would help to reduce the ecological cost
34 of industrial processes.

35 However, a large scattering of mechanical properties has been observed, in particular in the
36 distribution of rupture stress and Young's modulus of these fibres (Bourmaud et al., 2013;
37 Haag and Müssig, 2016; Lefeuvre et al., 2015; Shah et al., 2016), which could limits their
38 massive use for the design of structural or semi-structural composite material parts. Also,
39 unlike glass fibres, plant fibres such as flax and hemp have a non-linear mechanical behaviour
40 (Charlet, 2008; Cisse, 2016; Duval et al., 2011). To explain this variability and this complex
41 mechanical behaviour, the morphology, the biochemical composition and the microstructural
42 organization of elementary fibres or bundles are regularly discussed (Del Mastro et al., 2017;
43 Placet et al., 2014). Consequently, in-depth understanding of each of these parameters is
44 necessary to allow a more intensive and reliable use of these fibres in industrial processes.

45 Concerning the morphology, various studies have highlighted an important variability of
46 morphological characteristics of plant fibres. Experimental observations have clearly shown
47 that their cross-section is very irregular in size and shape (Charlet et al., 2007; Charlet, 2008;
48 Garat et al., 2018; Thuault, 2015) whereas for man-made fibres the cross-section is more

49 uniform. Moreover, in studies on plant fibres, the cross-section of the bundles is often
50 considered to be circular (Charlet, 2008; Cisse, 2016; Romão et al., 2004; Thuault, 2015). But
51 recent work has shown that the cross-section of flax and hemp bundles can be better assessed
52 by an elliptic model. Indeed, the simplified assumption of circular cross-section is suitable for
53 man-made fibre but lead to overestimate the CSA of flax and hemp fibre bundle (Garat et al.,
54 2018; Haag and Müssig, 2016). It is then clear that the geometric model used to represent the
55 cross-section in the calculations is of major importance and also influences the variability of
56 the mechanical properties of plant fibres (Aslan et al., 2011; Bourmaud et al., 2013; Ilczyszyn,
57 2013). Based on this observation, in this paper, we presented an elliptical model for a better
58 assessment of flax fibre bundle cross-section.

59 For the measurement of the CSA or the study of plant fibre morphology, there is no
60 standardised technique. Different methods are used by the authors: optical microscopy
61 (Charlet, 2008; Ilczyszyn, 2013; Yue et al., 2019), Scanning Electron Microscopy (Charlet,
62 2008; Thygesen et al., 2006), laser scan (Garat et al., 2018; Haag and Müssig, 2016),
63 Fraunhofer diffraction (Romão et al., 2004), X-ray tomography (Del Mastro et al., 2018) or
64 mathematical modelling combined with experimental data (Grishanov et al., 2006). In the
65 presented study, Fraunhofer diffraction has been chosen because – as non-destructive
66 technique using a laser beam – it allows the morphological study of a sample and the
67 subsequent mechanical testing of the same sample. Also, Fraunhofer diffraction requires less
68 time than tomography and therefore allows more samples to be analyzed.

69 The aim of our investigations is to study the morphological variations of flax fibre bundles
70 and to propose a non-destructive methodology to better assess the morphological
71 characteristics of plant fibres. Thanks to Fraunhofer diffraction, the inter-bundle variability of
72 cross-section and its lengthwise non-uniformity along bundle have been characterised and the
73 non-circularity of the cross-section was investigated by using an elliptical model to calculate

74 the CSA of the bundles. Furthermore, it is also known that the characterization of the 3D
75 morphology of plant fibres and in particular that of their bundles is a real challenge because of
76 the small size of these samples and the difficulties linked to experimental manipulations.
77 Based on our cross-section measurements, a numerical 3D reconstruction of external contour
78 of flax fibre bundle is finally proposed. The interest of such approach of three-dimensional
79 morphology is to propose a 3D model of a bundle respecting the dispersion of the measured
80 parameters. Also in further studies, by including elementary fibres in the bundle 3D
81 reconstructions as done by (Baley et al., 2018), these models can be introduced into a mesher
82 for finite element method studies that could help to improve the understanding of the
83 mechanics of flax fibre bundles.

84 **2. Materials and Methods**

85 **2.1. Materials**

86 The flax fibre bundles used to perform this morphological analysis were supplied by Natup
87 company and come from different flax varieties and batches. Since the origin of flax could
88 impact fibre bundles morphology and properties (Booth et al., 2004; Pisupati et al., 2021), a
89 batch of flax from the same origin could be used to exclude the influence of the plant variety.
90 Such specific study could be used in the futur with the methodology proposed here. The usual
91 treatment stages of plant fibres: retting, scutching and then combing were applied. **These**
92 **bundles have the particularity of having been treated with water spray, to make the natural**
93 **pectins more flexible and to use them as glue between millions of parallel bundles to form a**
94 **roll. For the purposes of the study, the bundles are randomly and manually extracted from the**
95 **roll. The extraction was done carefully to avoid bundle damage. A total of 100 fibre bundles**
96 **were characterized and their outer shape were reconstructed.**

97

98 **2.2. Method used to characterize the flax fibre bundle cross-section**

99 To determine the dimensions of the cross-sections, the Fraunhofer diffraction technique as
100 illustrated in **Figure 1a** was used. This technique consists in focusing a laser beam
101 (wavelength λ) on the cross-section to be characterized and collecting diffraction pattern
102 composed of several horizontal spots on a display table placed at a given distance D from the
103 fibre bundle. A visible green laser (class 3B, $\lambda = 532nm$, maximum power = 100mW) was
104 used for the tests.


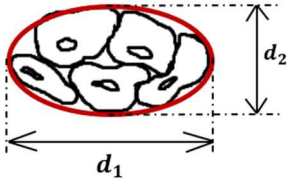
105 Each fibre bundle whose morphology is to be analysed is glued to a windowed cardboard
106 frame with a free length between the edges of 100 mm. According to (Lefeuvre, 2014), a
107 minimum of 6 measurements is required to have a sufficiently representative cross-section of
108 an elementary fibre. Despite the longer length of our samples, the same method was used in
109 the absence of more precise indication concerning the fibre bundles. Moreover, this number
110 of measurements per bundle allows us to optimize the experiment time as the number of
111 samples to be tested is high. Based on this assumption, along the free length of each bundle,
112 the dimensions of the cross-section are determined at 6 locations equidistant by 15 mm (15
113 mm, 30 mm, 45 mm, 60 mm, 75 mm, 90 mm).

114 Since the cross-section of fibre bundle is considered to be ellipsoidal in our investigations, the
115 axes (minor-axis and major-axis) d_1 and d_2 of the ellipse must then be determined to assure a
116 reliable elliptical CSA calculation (**Table 1**). In accordance to that geometry and the
117 mathematical definition of an ellipse, the axes d_1 and d_2 must be determined in two
118 orthogonal directions.

119 To achieve these goals, thanks to a device designed in the laboratory, the laser beam is first
120 focused on the point of the bundle whose cross-section is to be characterised and the width
121 δ_1 of the central diffraction spot on the display table is measured (**Figure 1b**).

122 Then, keeping the laser beam always focused on the same point, the support on which the
 123 cardboard is mounted is rotated by 90° around the longitudinal axis of the bundle and the
 124 width δ_2 of the central spot of the second diffraction pattern is also measured. The same
 125 operation is repeated for each of the 6 cross-sections along the bundle. This gives a total of
 126 twelve axis calculations per bundle. The two orthogonal directions named “Direction 1” and
 127 “Direction 2” are fixed in advance and are therefore identical for all samples.

128 **Table 1: Geometric model and formula used to calculate the CSA from diffraction**
 129 **measurements**

Real cross-section	Geometric model	CSA Calculation formula
		$CSA = \pi \times \frac{d_1}{2} \times \frac{d_2}{2} \quad (1)$

131
 132
 133
 134 **Figure 1: (a) Schematic diagram of the Fraunhofer diffraction principle and (b)**
 135 **Diffraction pattern recorded on the display table**

136 After recording the widths δ_1 et δ_2 , the axes d_1 and d_2 are then calculated using equation (2):

$$d = \frac{2D\lambda}{\delta} \quad (2)$$

137 with:

138 λ : laser beam wavelength

139 D: distance between the fibre bundle and the display table

140 δ : width of the central spot formed by the first two nodes of the diffraction pattern (**Figure**
141 **1b**)

142 The smallest axes between d_1 and d_2 is considered to be the minor-axis of the ellipse and the
143 largest one is considered to be the major-axis. Finally, the elliptical CSA is determined using
144 the equation (1) shown in the **Table 1**.

145 For scientific accuracy of later results discussion, it is useful here to recall some significant
146 consequences of the assumptions made about the cross-sections measurements:

- 147 - Since the measurement directions are taken randomly, it is not certain that the two
148 orthogonal dimensions measured correspond to the real axes (major and minor) of the
149 ellipse that would best fit the real cross-section. With the used method, the cross-
150 section is a projection in two orthogonal directions of the real cross-section.
- 151 - Using Fraunhofer diffraction, the disadvantage is that the measure neglects the lumens
152 of elementary fibres which form the bundle. The space occupied by the interfacial
153 lamella between elementary fibres is also not taken into account. However, knowing
154 that in a bundle cross-section, there are usually ten to forty elementary fibres, it
155 follows that the CSA calculated by neglecting the lumen and the interfacial lamella
156 will be slightly overestimated compared to the real CSA. We propose here an estimate
157 of the error made by neglecting the lumens.

158 Let us assume that at a given point, a bundle is composed of n elementary fibres. The CSA
159 measured at this point, neglecting the lumens is:

$$160 \quad CSA = \sum_{i=1}^n CSA_i \quad (3)$$

161 with:

162 CSA_i : the cross-section area of the elementary fibre of rank i measured by neglecting the area
163 of its lumen.

164 The real CSA of the bundle if the total area occupied by the lumens of the elementary fibres is
165 removed become:

$$166 \quad CSA' = \sum_{i=1}^n (1 - p_i) CSA_i \quad (4)$$

167 with:

168 p_i : the surface proportion occupied by the lumen of the elementary fibre of rank i .

$$169 \quad CSA' = \sum_{i=1}^n CSA_i - \sum_{i=1}^n p_i CSA_i \quad (4)$$

170

171 Since it is impossible for us to know the surface proportion of lumen for each elementary
172 fibre in a given cross-section of the bundle, we can take an average value from the literature
173 to estimate the overestimation caused by not taking lumens into account. Let's attribute this
174 average to all the fibres, in this case: $p_i = p$.

$$175 \quad CSA' = CSA - \sum_{i=1}^n p CSA_i \quad (4)$$

$$176 \quad CSA' = CSA - p \times \sum_{i=1}^n CSA_i \quad (4)$$

$$177 \quad CSA' = CSA - p \times CSA \quad (4)$$

$$178 \quad CSA' = (1 - p) CSA \quad (5)$$

179 Combining different studies (Charlet, 2008; Charlet et al., 2010; Richely et al., 2021), it
180 appears that on average the lumen area is between 0.4 and 10.5% of the CSA of the
181 elementary fibre. In this case the CSA of the bundle measured by neglecting only the lumens
182 of its elementary fibre would be on average overestimated by 0.4 to 10.5% compared to the
183 real CSA (calculated by taking into account the interfacial lamella between the elementary
184 fibres). This gives an idea of the overestimation of the cross-section area due to the
185 negligence of the lumens.

186 According to (Charlet et al., 2012) the length of the interfacial lamellae is between 5 μm and
187 15 μm and the thickness is about 0.5 μm . With such data, one could try to estimate a
188 theoretical surface proportion of the interfacial lamella, but the latter depends strongly on the
189 arrangement of the elementary fibres in a given section of the bundle. Therefore, an accurate
190 estimate will need the use of optical methods to measure on several samples: the CSA of a
191 bundle, the CSA of its constituent elementary fibres, the area of the lumens and the thickness
192 of the interfacial lamella between elementary fibres. This is beyond the scope of this work.
193 The mean of the 6 calculated CSAs of the bundle was taken as its representative mean CSA:
194 CSA_{EM} . In total we characterised 100 bundles. For 7 of these bundles, however, the
195 measurements were carried out at 5 points due to elementary fibre detachments along the
196 bundle resulting in 593 cross-sections measurements.

197 **3. Results and discussion**

198 **3.1.Scattering of flax fibre bundle axes**

199 With 593 cross-sections characterized by two axes d_1 and d_2 , there are a total of 1186
200 measurements. Analysis of the results reveals a large scattering of the axes with **respectively a**
201 **mean value of $104\pm 38 \mu\text{m}$ for minor-axis and $158\pm 54 \mu\text{m}$ for major-axis (Figure 2a and 2b).**
202 The distribution of the axes was characterised by testing different statistical distribution laws
203 using the Anderson-Darling test implemented in Matlab software. Only the log-normal
204 distribution (6) seems to be suitable for the distribution of the axes (** $P\leq 0.01$).

$$205 \quad \text{Log}(\mu, \sigma) : f(x) = \frac{1}{x\sigma\sqrt{2\pi}} \exp\left[-\frac{((\ln x)-\mu)^2}{2\sigma^2}\right] \quad (6)$$

206 with:

207 μ and σ the parameters of the log-normal distribution

208

209 This large scattering is quite characteristic of plant fibres because they grow in natural
210 conditions which imply a heterogeneity of their cross-section dimensions, unlike man-made

211 fibres whose dimensions can be standardised during their industrial production. Compared to
212 other studies on “flax fibre bundle apparent diameter”, the mean value of our calculated axes
213 is higher than that obtained by (Haag and Müssig, 2016) and (Garat et al., 2018). Apart from
214 natural causes, the significantly higher length of the bundles tested in our case and the number
215 of cross-sections analysed may be the cause of this discrepancy. This difference may also be
216 due to the treatments applied to the fibre bundles used in the different studies. Harvesting and
217 processing conditions can also influence the geometry of these fibres. Indeed, the more the
218 bundles undergo individualization operations – according to the use that will be made of them
219 – the more the number of elementary fibres per bundle decreases, thus lowering the
220 dimensions of the resulting bundle.

221 Furthermore, it should be noted that other factors such the measurement technique accuracy
222 can also influence the results of calculated cross-section dimensions of plant fibres. In fact,
223 for the same batch of flax bundles, the difference in technique used to measure the cross-
224 section dimensions can lead to an error of up to 175% in the calculation of the tensile stress,
225 due to the bias introduced by each technique (automated laser, microscopy, flat-bed scanning)
226 in the measure (Haag and Müssig, 2016).

227 Simultaneous lengthwise evolution of some bundle axis dimension highlights the non-
228 circularity of the cross-section (**Figure 2c**). This clearly shows that when the cross-section is
229 considered circular, the “mean apparent diameter” of the bundle which will be calculated will
230 depend on the direction of measurement. For the batch of 100 bundles the relative difference
231 between the two “mean apparent diameters” calculated according to Direction 1 and Direction
232 2 (considering the cross-section to be a circle of diameter d_1 in Direction 1 or d_2 in Direction
233 2) respectively is around $20 \% \pm 17$. This implies that the mechanical properties which will be
234 obtained using each of “mean apparent diameter” will be impacted by this difference. The

235 random measurement angle of characterisation chosen by the experimenter is hence a source
 236 of variability reported by many studies (Aslan et al., 2011; Bourmaud et al., 2013) in both the
 237 cross-section dimensions calculation and the mechanical properties that will be attributed to
 238 the bundle. Indeed, the rupture stress and Young's modulus depend directly on the mean CSA
 239 of the bundle. This conclusion is obviously valid for elementary fibres.

Figure 2: Characteristics of the axes of the cross-section: (a) Distribution of the minor-axes, (b) Distribution of the major-axes and (c) Lengthwise evolution of cross-section axis for two bundles

240

241 **3.2. Scattering and lengthwise variation of CSA along the bundle**

242 The 593 cross-sections calculated from the axis measurements were analysed and again
 243 revealed a large variability inherent to plant fibres. This cross-section scattering is the logical
 244 consequence of the axis scattering discussed in **section 3.1**. In terms of distribution, the cross-
 245 section distribution also follows a log-normal distribution (*P≤0.05) (**Figure 3a**).

246 **Table 2: Calculated geometric parameters of flax fibre bundles CSA**

	Min	~Mean	Max
CSA (μm^2)	836	14062	68267
Minor-axis (μm)	27.8	121.7	251.4
Major-axis (μm)	38.3	147.2	345.9

247

248 The mean CSA is $13947 \pm 9331 \mu\text{m}^2$. Our results are quite similar to those of (Charlet,
 249 2008) who found respectively on two different batches of bundles, mean CSA of $14107 \pm$
 250 $4555 \mu\text{m}^2$ and $13881 \pm 4496 \mu\text{m}^2$ by image analysis. On the other hand, compared to the
 251 mean CSA of $6148 \mu\text{m}^2$ found by (Garat et al., 2018) using optical microscopy, the mean
 252 cross-section of this present study is more than the double. To explain the important

253 difference with the results of (Garat et al., 2018), one can mention again the origin of samples
254 and the individualisation processes they underwent before being characterised. In fact, it is
255 really difficult to conclude on this point because few precise indications are given on this
256 information in the different publications. The variety of flax used in the studies may also be
257 the source of this high difference. But it is unlikely in the light of our knowledge that the
258 difference in variety can justify such a large difference. (Thuault, 2015) studied the “apparent
259 diameters” of seven varieties of flax and concluded from his statistical results that there is no
260 significant different between diameter from one variety to another.

261 There is also strong intra-bundle heterogeneity in the cross-sections. The characterisation of
262 this heterogeneity is crucial to set-up the 3D outer contour of the bundles. Here, two levels of
263 study are required: on the one hand, the evolution of the size (CSA) of the cross-section and,
264 on the other, the evolution of its shape. In the actual section, the first level of the study is
265 discussed. For a sample, the cross-section heterogeneity ratio r_s – which represents the
266 multiplication factor of the CSA over 75 mm (15 mm to 90 mm) – is calculated by equation
267 (7). It is worth noting that this ratio is computed for each of the six sections of the bundle:

$$268 \quad r_s = \frac{\max(CSA_i)}{\min(CSA_i)} \quad i = 1; 2 \dots; 6$$

269 (7)

270 On average the CSA is multiplied by 3.4 over 75 mm. **Table 3** gives the r_s values for 10
271 representative samples from the batch of 100 bundles characterised. The ratio of the
272 maximum CSA to the minimum CSA can reach values of the order of ten. However, it should
273 be noted that 90% of the r_s values are below 6. Despite the small number of measurement
274 points compared to the length of our samples, this result shows the high variability of CSA
275 along the bundle (**Figure 3b**). This variation in cross-section can cause stress concentrations
276 that would add to the elementary inter-fibre friction that occurs in a tensile test on a plant
277 fibre bundle. Once again, the CSA scattering is one of the reasons which could explain the
278 scattering of mechanical properties since each bundle has a unique morphology that

279 influences its mechanical properties whatever the sample length, notably through the
 280 calculation of the mean CSA.

Figure 3: (a) Cross-Section Area distribution and (b) Lengthwise variations of flax fibre bundle CSA

281

282

283 The explications of this CSA lengthwise variation can be multiple. As the elementary fibres
 284 are not continuous and given the length of the bundles tested, the number of elementary fibres
 285 per cross-section is very likely to be different. This would result in CSA high variations. Even
 286 if between two measuring points, the number of elementary fibres would be identical, the
 287 consistency of the CSA is not at all guaranteed.

Table 3: Analysis of CSA heterogeneity for 10 representative bundles of the total batch

289

Bundle	L1	L2	L3	L4	L5	L6	L7	L8	L9	L10
Mean CSA (μm^2)	10288	15917	16250	15461	15567	10322	8998	8215	29975	14875
Standard-deviation	1277	5086	5780	9612	10419	6729	6231	6899	22946	13368
r_s	1.4	2.2	3.5	4.1	5.4	6.7	7.2	8.6	9.2	12.0

290

291 It should be remembered here that even elementary fibre do not have a constant CSA
 292 (Charlet, 2008; Thuault, 2015). Using a camera equipped with lenses that can see details at
 293 the micrometer scale, the bundles were photographed to highlight these strong lengthwise
 294 variations of the CSA (**Figure 4**).

Figure 4: Two different flax fibre bundles section seen in profile

296 Let now d_{1m} ou d_{2m} be the mean axes of the bundle in the Direction 1 and Direction 2
 297 respectively. A power regression correlation law between the “maximum mean axis” $d_m =$

298 $\max(d_{1m}, d_{2m})$ and the mean elliptical cross-section area CSA_{EM} of the bundle was
299 developed (**Figure 5a**):

$$300 \quad CSA_{EM} = k \times d_m^n \quad (8)$$

301 When the “maximum mean axis” is less than 100 μm , the calculated mean elliptical CSA
302 given by the power law given in equation (8) is very close to the experimental results. This
303 law deviates from calculated mean elliptical CSA for high “maximum mean axis”.

304 **3.3. Ellipticity of flax fibre bundle cross-section**

305 The measurements also confirm the ellipticity of the cross-sections. For each of the 593 cross-
306 sections, the ellipticity e is calculated to better characterization of the cross-section shape (9):

$$307 \quad e = 1 - \frac{\min(d_1, d_2)}{\max(d_1, d_2)} = 1 - \frac{\text{minor-axis}}{\text{major-axis}} \quad (9)$$

308 From a mathematical point of view, this definition makes it possible to identify the flattening
309 degree of an elliptical curve. The more circular the characterized cross-section is, the more e
310 tends towards 0 since in this case d_1 and d_2 are quite close. Otherwise, the flatter the ellipse
311 corresponding to the cross-section is, the more e tends towards 1. With a range of values
312 from 0 to 0.77, the distribution the ellipticity is highly random compared to those of axes and
313 cross-sections. The mean ellipticity is 0.32 and confirms the relevance of the elliptical model
314 for determining the CSA of flax fibre bundles. On the basis of this result, it can therefore be
315 concluded that, compared to the circular model, the elliptical model seems to be more suitable
316 for determining the CSA of flax fibre bundles.

317 The comparison with other similar works (Garat et al., 2018; Haag and Müssig, 2016) on
318 plant fibre shape requires the calculation of the shape factor f defined as ratio between the
319 major and minor axis of the ellipse:

$$320 \quad f = \frac{\max(d_1, d_2)}{\min(d_1, d_2)} \quad (10)$$

321 It was found for all 593 cross-sections: $f_{mean} = 1.6$, $f_{min} = 1$ et $f_{max} = 4.3$. Our result is
322 similar to that of (Haag and Müssig, 2016) for whom the f_{mean} is 1.76. but lower than the
323 value of 2.58 found by (Garat et al., 2018) for fibre bundle cross-sections. Nevertheless, the
324 three studies lead to the same conclusion: the cross-section of flax fibre bundles is rather
325 elliptical. The ellipse corresponding to the mean shape factor f_{mean} of the present study is
326 drawn on the **Figure 5b** in comparison with a circle whose diameter would be the major axis
327 of the ellipse. The flattening degree of the ellipse close to the real cross-section clearly
328 illustrates the non-circularity of the flax fibre bundle.

329 The second level of study required to perform the 3D reconstruction of the bundle outer
330 contour is the lengthwise evolution of the cross-section shape. The analysis of the intra-
331 bundle heterogeneity shows that the shape factor doubles on average over 75 mm. Not only
332 can the CSA be multiplied by 3.4 over 75 mm, but the cross-section shape factor can be
333 multiplied by 2 on average. These results illustrate the important irregularity exhibited by the
334 morphology of flax fibre bundles.

**Figure 5: (a) Power law correlation between “maximum mean axis” and mean CSA of
the bundle and (b) Illustration of the ellipticity of flax fibre bundle : curves drawn with
major axis of the ellipse = diameter of the comparison circle = 100 μ m**

335

336 Although the study of the influence of the geometrical model used to calculate the CSA on the
337 mechanical properties is beyond the scope of this works, these findings confirms that the
338 geometric model directly influences the mechanical properties of the sample (Aslan et al.,
339 2011). For example, in our case, when the mean cross-section of the bundle is calculated by
340 considering a circular cross-section (assuming that the cross-section is a circle of diameter d_1
341 in Direction 1 or d_2 in Direction 2), there is an average overestimation of 12% compared to
342 the mean cross-section calculated using the elliptical model. Therefore, as suggested by (Virk,

2010), if the circular model is used when measuring cross-section, it would be relevant to determine a “correction factor” for the CSA to take into account the overestimation induced by the geometrical model. This correction factor, which according to our study would be the mean shape factor of 1.6 for flax bundle, is slightly lower than the value of 1.76 proposed by (Haag and Müssig, 2016) but greater than the value of 1.42 proposed for jute fibre bundles by (Virk, 2010).

3.4. Possible rotation of the cross-section along the fibre bundle

The lengthwise evolution of the cross-section has been finely analysed and it was noted that the orientation of the major axis of the ellipse can be different from one cross-section to another. Indeed, for each of the cross-sections, we named d_1 the axis measured along Direction 1 and d_2 the one measured along Direction 2. Considering 2 consecutive cross-sections and assuming that for the first one $d_1 > d_2$ there is no guarantee that in the second cross-section we will have $d_1 > d_2$ but rather the opposite. When this reasoning is extended to each pair of consecutive cross-sections, according to our method of measurements, the orientation of the cross-section can be different from one point to another (**Figure 6a**).

For the 100 bundles, this change in cross-section orientation between two consecutive points occurs on average 2 times when considering 75 mm over a bundle. As evidence of this, we have taken high precision pictures of bundles, where it is clear that some bundles are twisted (**Figure 6b**).

362

Figure 6: (a) Illustration of the change of orientation between two consecutive sections

and (b) Bundle with local twisting

Using Fraunhofer diffraction or any other laser technique, the number of measurement points per cross-section and per bundle would have to be increased to get an average value closer to reality. The results of our study are indicative since – as we have already reminded – the

368 ellipse by which we assessed the cross-section corresponds to a view along two orthogonal
369 directions. The change of orientation observed can have several origins according to the
370 following two scenarios. Since a bundle is an assembly of discontinuous elementary fibres,
371 this change in the orientation of the cross-section may be due to the difference in the
372 arrangement of the elementary fibres between two consecutive points (**Figure 7a**). In other
373 words, depending on the appearance and disappearance of the elementary fibres, the
374 orientation of the cross-section considered as an ellipse could change. In this case, there
375 would be no twisting of the bundle, but just a change in orientation corresponding to the
376 ellipse that best approximates the cross-section. If two consecutive cross-sections of a bundle
377 have an elementary fibre arrangement, as shown in the **Figure 7a**, it is clear that the
378 orientation of the major-axis of the ellipse corresponding to the cross-section changes
379 between Cross-Section i and Cross-Section $i+1$. Our calculation method would in this case
380 show a twisting when there is no twisting but only a different disposition of elementary fibre.
381 The other possible scenario is that the growth conditions of the bundles in flax stem or the
382 processing conditions may have favoured an irregular evolution of the orientation of the
383 cross-sections, thus causing twisting along the bundle. Furthermore, the scenario of a bundle
384 of fibres which twists himself after combing should not be a surprise if all the microfibril
385 helices – which act at the main rigid elements inside elementary fibre – are orientated in the
386 same direction (S-helice) (Baley, 2002; Bergfjord and Holst, 2010). In that case, it can be
387 hypothesized that the twisting is due to stress relaxation once the bundle is released. As the
388 microfibrillar angle is much higher in defect areas such as kink-bands than in the rest of the
389 flax fibres (Melelli et al., 2021), it is conceivable that a difference in relaxation ratio may
390 induce or increase such twisting. This twisting revealed by the numerical analysis and the
391 optical observations would probably explain the rotation of the bundle at the beginning of the

392 tensile load observed by (Ahmed and Ulven, 2018) using in-situ Scanning Electron
393 Microscopy.

394 **3.5. 3D reconstruction of flax fibre bundles outer contour**

395 The knowledge of the exact morphology of plant fibre bundles and its lengthwise evolution is
396 a very important issue. Indeed, more and more studies are focusing on the propagation of the
397 mechanical behaviour of elementary fibre to the bundle. When performing numerical
398 simulations of bundle mechanical behaviour, taking into the account the disposition of
399 elementary fibres in a circle or ellipse can have an influence on the resulting behaviour of the
400 bundle. For example, numerical simulations by (Del Mastro et al., 2017) have shown that the
401 more the ellipticity of a hemp elementary fibre tends towards 0, the more the tensile
402 behaviour of the fibre is non-linear. In addition, a better knowledge of bundle morphology
403 could allow an in-depth study of the effect of twisting on their mechanical behaviour. It is
404 quite possible that there is a mechanical coupling (tensile-torsion) or high stress-concentration
405 during the elongation of these samples. Due to the size of the bundle or elementary fibre the
406 fine description of the morphology remains little investigated. To overcome this experimental
407 difficulty, numerical approaches are increasingly being considered (Mattrand et al., 2014;
408 Ntenga and Beakou, 2011) and make it possible to study the relationship between the
409 complex morphology of plant fibres and their mechanical behaviour (Del Mastro et al., 2017).
410 So, based on the results of our morphological analysis, the outer contour of the fibre bundles
411 as made possible by our measurement method was reconstructed numerically. The following
412 basic assumptions are made:

413 - In accordance with the model adopted for our measurements, the cross-section is
414 assumed to be elliptical and the bundle is assumed to have perfect symmetry around its
415 longitudinal axis.

416 - The morphology reconstructed ignores the disposition of elementary fibres which
417 constitute the bundles. So the bundle is considered as a homogeneous medium.
418 Three types of bundles were reconstructed (**Figure 7b, 7c and 7d**): a bundle with little
419 morphological variation; a bundle with strong morphological variations, and a bundle
420 reconstructed with mean lengthwise evolution of the cross-section.

Figure 7: (a) Example of elementary fibre disposition which could induce a change of orientation of the cross-section according to our calculation method, (b) 3D reconstruction of the outer contour of bundle with little morphological variation, c) 3D reconstruction of the outer contour of bundle with strong morphological variations, d) A 3D reconstructed bundle with the average values of lengthwise evolution of the cross-section and e) 3D reconstruction of a bundle outer contour by X-ray nanotomography (Del Masto, 2018)

It is possible to compare this purely numerical 3D reconstruction by X-ray nanotomography 3D reconstruction of a bundle outer contour (**Figure 7e**). Note that the number of characterized cross-sections per bundle should be increased to approach more realistic description. However, the heterogeneity of the cross-section highlighted by the measurements is well illustrated in these reconstructions. The models obtained here will be refined and can be used to study by numerical simulations the relationship between the complex morphology of bundles and their tensile behaviour.

421 **4. Conclusion**

422 In this paper, we investigated the morphological variations of flax fibre bundles cross-section
423 using the Fraunhofer diffraction technique. A particular focus was made on the heterogeneity
424 of the morphology of a hundred flax fibre bundles. The first finding is the confirmation of the
425 high intra-bundle and inter-bundle scattering of the cross-section. Over 75 mm of a 100 mm

426 length bundle, the cross-section area (CSA) is on average multiplied by 3.4 and the shape
427 factor of cross-section doubles. This clearly shows that it is imperative to determine a mean
428 CSA per bundle for later calculation of mechanical properties. Our method has also
429 highlighted the elliptical shape of the bundles cross-sections. Compared to the elliptical
430 model, using a circular model to obtain an “mean apparent diameter” of the bundle is a less
431 relevant method for a reliable estimation of flax fibre bundles CSA.

432 The morphological scattering coupled with the method geometrical model of the cross-section
433 & measurement technique) used to characterize the cross-sections is one of the reasons which
434 explain the dispersion of the mechanical properties reported by different studies on flax fibre
435 bundles. A standardisation of the method using to determine the CSA of plant fibres is
436 strongly required to eliminate the variability introduced by the different techniques used. This
437 would allow a more reliable comparison of results from different studies. The method
438 proposed here for plant fibres is of particular interest if it is essential that the analysed
439 samples keep their morphology undamaged for further testing.

440 Additionally, a possible change in cross-section orientation between two consecutive
441 measurement points along the bundle was revealed. Local twisting of some bundles was thus
442 observed. More detailed analyses, such as an increase in the number of measurement points
443 per cross-section and per – which is possible with automated laser scanning device – would
444 be needed to gain in-depth knowledge of these local bundle twists.

445 These different results allowed us to reconstruct the 3D evolution of the outer contour of flax
446 fibre bundles. Although performed numerically with a low number of cross-sections per
447 bundle given the length of our samples, the reconstruction helps to highlight the significant
448 heterogeneity in the size and shape of the flax fibre bundle cross-section. In future works, by
449 incorporating elementary fibres in the 3D reconstructions, the use of finite element method
450 could help to better understand the mechanical behaviour of the bundles: especially stress

451 concentration phenomena and the shear occurring at the interface of elementary fibres during a
452 tensile test.

453

454 **Funding:** This research did not receive any specific grant from funding agencies in the
455 public, commercial, or not-for-profit sectors.

456

457

458

459

460

461

462 **References**

463 Ahmed, S., Ulven, C.A., 2018. Dynamic in-situ observation on the failure mechanism of flax
464 fiber through scanning electron microscopy. *Fibers* 6.
465 <https://doi.org/10.3390/FIB6010017>

466 Aslan, M., Chinga-Carrasco, G., Sørensen, B.F., Madsen, B., 2011. Strength variability of
467 single flax fibres. *J. Mater. Sci.* 46, 6344–6354. <https://doi.org/10.1007/s10853-011-5581-x>

469 Baley, C., 2002. Analysis of the flax fibres tensile behaviour and analysis of the tensile
470 stiffness increase. *Compos. - Part A Appl. Sci. Manuf.* 33, 939–948.
471 [https://doi.org/10.1016/S1359-835X\(02\)00040-4](https://doi.org/10.1016/S1359-835X(02)00040-4)

472 Baley, C., Goudenhoft, C., Gibaud, M., Bourmaud, A., 2018. Flax stems: From a specific
473 architecture to an instructive model for bioinspired composite structures. *Bioinspiration and Biomimetics* 13, aaa6b7. <https://doi.org/10.1088/1748-3190/aaa6b7>

475 Bledzki, A.K., Gassan, J., 1999. Composites reinforced with cellulose based fibres. *Prog.*
476 *Polym. Sci.* 24, 221–274. [https://doi.org/10.1016/S0079-6700\(98\)00018-5](https://doi.org/10.1016/S0079-6700(98)00018-5)

477 Booth, I., Harwood, R.J., Wyatt, J.L., Grishanov, S., 2004. A comparative study of the
478 characteristics of fibre-flax (*Linum usitatissimum*). *Ind. Crops Prod.* 20, 89–95.
479 <https://doi.org/10.1016/j.indcrop.2003.12.014>

480 Bourmaud, A., Morvan, C., Bouali, A., Placet, V., Perré, P., Baley, C., 2013. Relationships
481 between micro-fibrillar angle, mechanical properties and biochemical composition of
482 flax fibers. *Ind. Crops Prod.* 44, 343–351. <https://doi.org/10.1016/j.indcrop.2012.11.031>

483 Charlet, K., 2008. Contribution à l'étude de composites unidirectionnels renforcés par des
484 fibres de lin : relation entre la microstructure de la fibre et ses propriétés mécaniques.
485 <https://doi.org/...>

486 Charlet, K., Baley, C., Morvan, C., Jernot, J.P., Gomina, M., Bréard, J., 2007. Characteristics
487 of Hermès flax fibres as a function of their location in the stem and properties of the
488 derived unidirectional composites. *Compos. Part A Appl. Sci. Manuf.* 38, 1912–1921.
489 <https://doi.org/10.1016/j.compositesa.2007.03.006>

490 Charlet, K., Gaillard-Martinie, B., Béakou, A., 2012. Comportement mécanique et
491 modélisation numérique de la lamelle mitoyenne de lin. *Ann. Chim. Sci. des Mater.* 37,
492 341–350. <https://doi.org/10.3166/RCMA.22.341-350>

493 Charlet, K., Jernot, J.P., Eve, S., Gomina, M., Bréard, J., 2010. Multi-scale morphological
494 characterisation of flax: From the stem to the fibrils. *Carbohydr. Polym.* 82, 54–61.
495 <https://doi.org/10.1016/j.carbpol.2010.04.022>

496 Cisse, O., 2016. Caractérisation du comportement hygro-mécanique des fibres libériennes
497 élémentaires issues du chanvre. PhD Thesis, Université de Franche-Comté, France.

498 Del Mastro, A., Trivaudey, F., Guicheret-Retel, V., Placet, V., Boubakar, L., 2017. Nonlinear
499 tensile behaviour of elementary hemp fibres: a numerical investigation of the
500 relationships between 3D geometry and tensile behaviour. *J. Mater. Sci.* 52.
501 <https://doi.org/10.1007/s10853-017-0896-x>

502 Del Mastro, A., 2018. Transition d'échelle entre fibre végétale et compositeUD : propagation
503 de la variabilité et des non-linéarités. PhD Thesis, Université de Bourgogne Franche-
504 Comté, France.

505 Dicker, M.P.M., Duckworth, P.F., Baker, A.B., Francois, G., Hazzard, M.K., Weaver, P.M.,
506 2014. Green composites: A review of material attributes and complementary
507 applications. *Compos. Part A Appl. Sci. Manuf.* 56, 280–289.
508 <https://doi.org/10.1016/j.compositesa.2013.10.014>

509 Duval, A., Bourmaud, A., Augier, L., Baley, C., 2011. Influence of the sampling area of the
510 stem on the mechanical properties of hemp fibers. *Mater. Lett.* 65, 797–800.
511 <https://doi.org/10.1016/j.matlet.2010.11.053>

512 Garat, W., Corn, S., Le Moigne, N., Beaugrand, J., Bergeret, A., 2018. Analysis of the
513 morphometric variations in natural fibres by automated laser scanning: Towards an
514 efficient and reliable assessment of the cross-sectional area. *Compos. Part A Appl. Sci.*
515 *Manuf.* 108, 114–123. <https://doi.org/10.1016/j.compositesa.2018.02.018>

516 Goda, K., Cao, Y., 2007. Research and Development of Fully Green Composites Reinforced
517 with Natural Fibers. *J. Solid Mech. Mater. Eng.* 1, 1073–1084.
518 <https://doi.org/10.1299/jmmp.1.1073>

519 Grishanov, S.A., Harwood, R.J., Booth, I., 2006. A method of estimating the single flax fibre
520 fineness using data from the LaserScan system. *Ind. Crops Prod.* 23, 273–287.
521 <https://doi.org/10.1016/j.indcrop.2005.08.003>

522 Haag, K., Müssig, J., 2016. Scatter in tensile properties of flax fibre bundles: influence of
523 determination and calculation of the cross-sectional area. *J. Mater. Sci.* 51, 7907–7917.
524 <https://doi.org/10.1007/s10853-016-0052-z>

525 Ilczyszyn, F., 2013. Caractérisation expérimentale et numérique du comportement mécanique
526 des agro-composites renforcés par des fibres de chanvre 385. PhD Thesis. Université de

527 Technologie de Troyes, France.

528 Joshi, S. V., Drzal, L.T., Mohanty, A.K., Arora, S., 2004. Are natural fiber composites
529 environmentally superior to glass fiber reinforced composites? *Compos. Part A Appl.*
530 *Sci. Manuf.* 35, 371–376. <https://doi.org/10.1016/j.compositesa.2003.09.016>

531 Lefeuvre A., 2014. Contribution à l'étude des propriétés des fibres de lin (*Linum*
532 *Usitatissimum*, variétés Marilyn et Andréa) en fonction des pratiques culturales sur le plateau
533 du Neubourg. Fibres destinées au renforcement de matériaux composites". PhD Thesis,
534 Université de Rouen, France.

535 Lefeuvre, A., Duigou, A. Le, Bourmaud, A., Kervoelen, A., Morvan, C., Baley, C., 2015.
536 Analysis of the role of the main constitutive polysaccharides in the flax fibre mechanical
537 behaviour. *Ind. Crops Prod.* 76, 1039–1048.
538 <https://doi.org/10.1016/j.indcrop.2015.07.062>

539 Mattrand, C., Béakou, A., Charlet, K., 2014. Numerical modeling of the flax fiber
540 morphology variability. *Compos. Part A Appl. Sci. Manuf.* 63, 10–20.
541 <https://doi.org/10.1016/j.compositesa.2014.03.020>

542 Melelli, A., Durand, S., Arnould, O., Richely, E., Guessasma, S., Jamme, F., Beaugrand, J.,
543 Bourmaud, A., 2021. Extensive investigation of the ultrastructure of kink-bands in flax
544 fibres. *Ind. Crops Prod.* 164. <https://doi.org/10.1016/j.indcrop.2021.113368>

545 Ntenga, R., Beakou, A., 2011. Structure, morphology and mechanical properties of
546 *Rhctophyllum camerunense* (RC) plant-fiber. Part I: Statistical description and image-
547 based reconstruction of the cross-section. *Comput. Mater. Sci.* 50, 1442–1449.
548 <https://doi.org/10.1016/j.commatsci.2010.11.032>

549 Pisupati, A., Willaert, L., Goethals, F., Uyttendaele, W., Park, C.H., 2021. Variety and
550 growing condition effect on the yield and tensile strength of flax fibers. *Ind. Crops Prod.*
551 170, 113736. <https://doi.org/10.1016/j.indcrop.2021.113736>

552 Placet, V., Cissé, O., Lamine Boubakar, M., 2014. Nonlinear tensile behaviour of elementary
553 hemp fibres. Part I: Investigation of the possible origins using repeated progressive
554 loading with in situ microscopic observations. *Compos. Part A Appl. Sci. Manuf.* 56,
555 319–327. <https://doi.org/10.1016/j.compositesa.2012.11.019>

556 Richely, E., Durand, S., Melelli, A., Kao, A., Magueresse, A., Dhakal, H., Gorshkova, T.,
557 Callebert, F., Bourmaud, A., Beaugrand, J., Guessasma, S., 2021. Novel insight into the
558 intricate shape of flax fibre lumen. *Fibers* 9, 1–17. <https://doi.org/10.3390/fib9040024>

559 Romão, C., Vieira, P., Peito, F., Marques, A.T., Esteves, J.L., 2004. Single filament
560 mechanical characterisation of hemp fibres for reinforcing composite materials. *Mol.*
561 *Cryst. Liq. Cryst.* 418. <https://doi.org/10.1080/15421400490479172>

562 Shah, D.U., Nag, R.K., Clifford, M.J., 2016. Why do we observe significant differences
563 between measured and ‘back-calculated’ properties of natural fibres? *Cellulose* 23,
564 1481–1490. <https://doi.org/10.1007/s10570-016-0926-x>

565 Thuault, A., 2015. Approche multi-échelle de la structure et du comportement mécanique de
566 la fibre de lin. PhD Thesis, Université de Caen Basse Normandie, France.

567 Thygesen, L.G., Bilde-Sørensen, J.B., Hoffmeyer, P., 2006. Visualisation of dislocations in
568 hemp fibres: A comparison between scanning electron microscopy (SEM) and polarized
569 light microscopy (PLM). *Ind. Crops Prod.* 24, 181–185.
570 <https://doi.org/10.1016/j.indcrop.2006.03.009>

571 Virk, A.S., 2010. Numerical models for natural fibre composites with stochastic properties.
572 PhD Thesis, Plymouth University, England. [https://pearl.ply-](https://pearl.plymouth.ac.uk/handle/10026.1/517)
573 [mouth.ac.uk/handle/10026.1/517](https://pearl.plymouth.ac.uk/handle/10026.1/517).

574 Wambua, P., Ivens, J., Verpoest, I., 2003. Natural fibres: Can they replace glass in fibre
575 reinforced plastics? *Compos. Sci. Technol.* 63, 1259–1264.
576 [https://doi.org/10.1016/S0266-3538\(03\)00096-4](https://doi.org/10.1016/S0266-3538(03)00096-4)

577 Yan, L., Chouw, N., Jayaraman, K., 2014. Flax fibre and its composites - A review. *Compos.*
578 *Part B Eng.* 56, 296–317. <https://doi.org/10.1016/j.compositesb.2013.08.014>
579 Yue, H., Rubalcaba, J.C., Cui, Y., Fernández-Blázquez, J.P., Yang, C., Shuttleworth, P.S.,
580 2019. Determination of cross-sectional area of natural plant fibres and fibre failure
581 analysis by in situ SEM observation during microtensile tests. *Cellulose* 26, 4693–4706.
582 <https://doi.org/10.1007/s10570-019-02428-7>
583

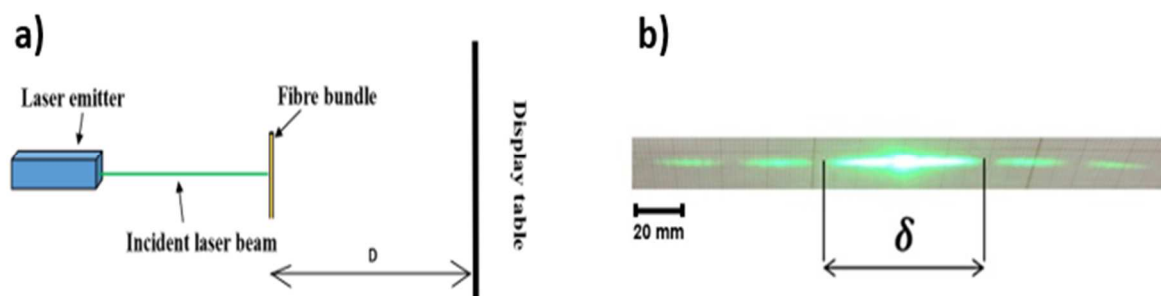
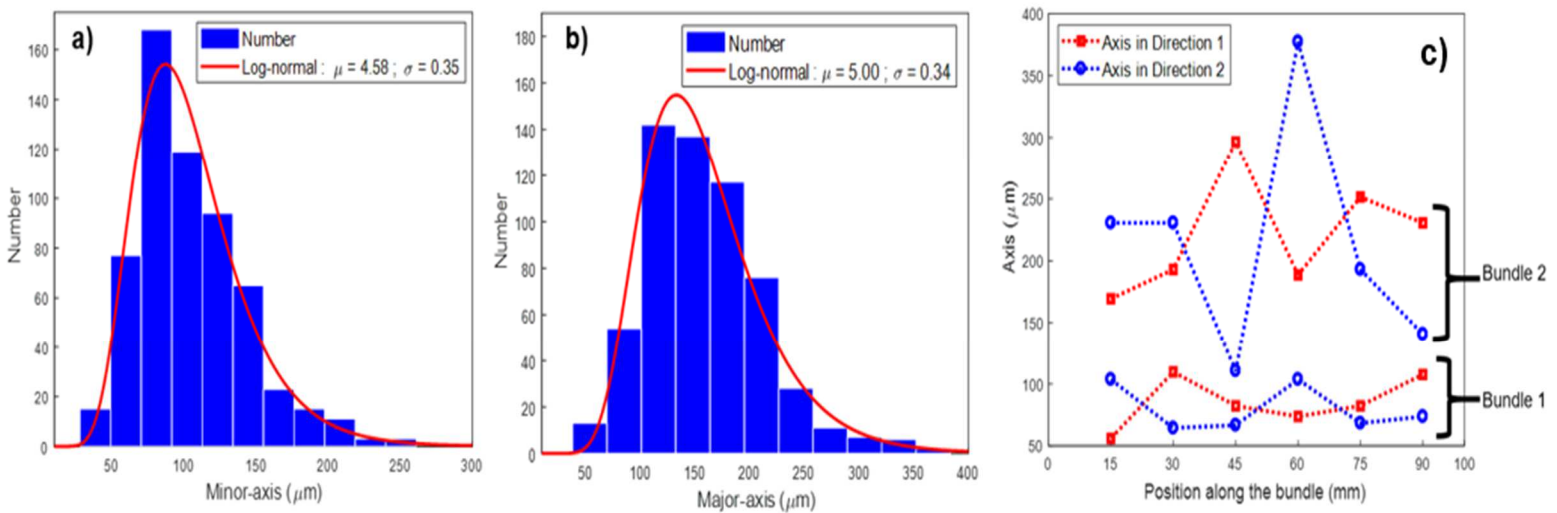
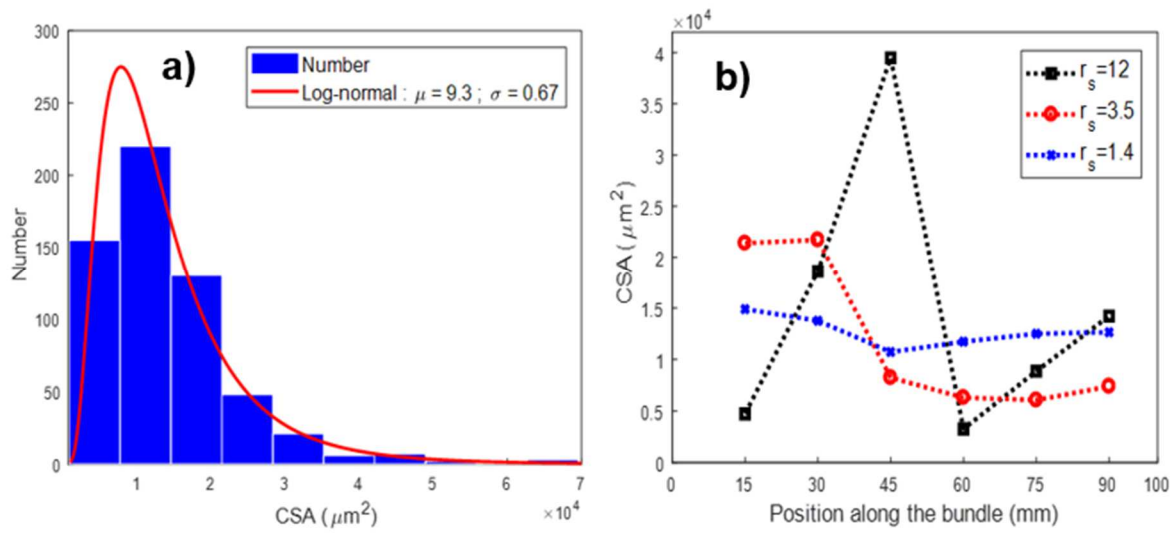


Figure 1: (a) Schematic diagram of the Fraunhofer diffraction principle and (b) Diffraction pattern recorded on the display table

584
585

Figure 2: Characteristics of the axes of the cross-section: (a) Distribution of the minor-axes, (b) Distribution of the major-axes and (c) Lengthwise evolution of cross-section axis for two bundles





587 **Figure 3: (a) Cross-Section Area distribution and (b) Lengthwise variations of flax fibre**
 588 **bundle CSA**

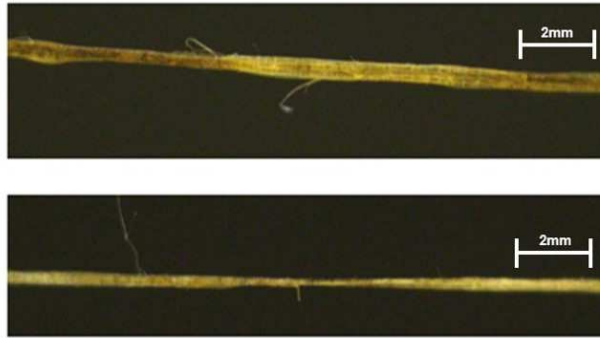
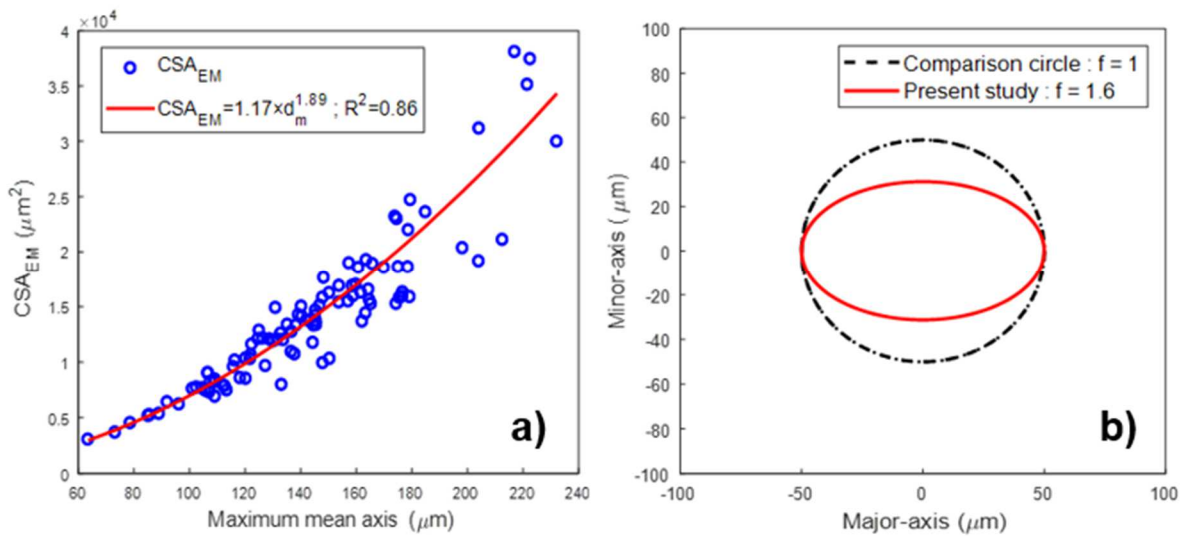
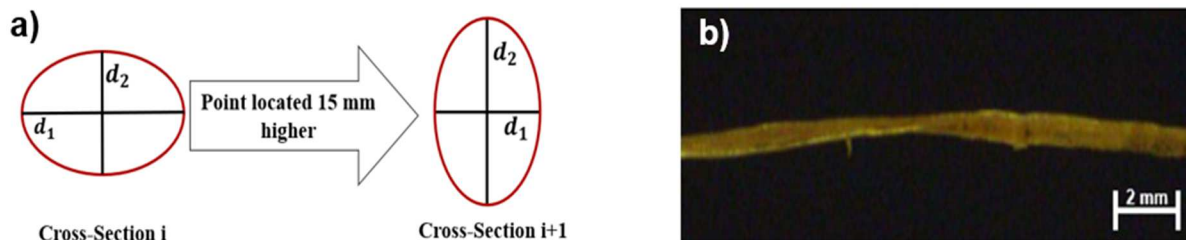


Figure 4: Two different flax fibre bundles section seen in profile

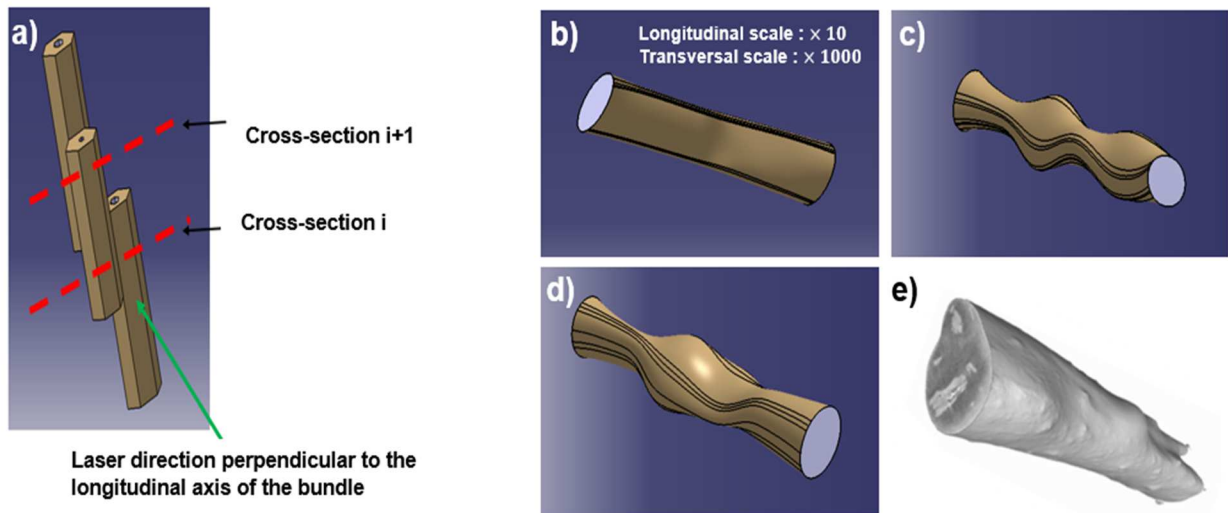


589

590 Figure 5: (a) Power law correlation between “maximum mean axis” and mean CSA of
 591 the bundle and (b) Illustration of the ellipticity of flax fibre bundle : curves drawn with
 592 major axis of the ellipse = diameter of the comparison circle = 100 μm



593 Figure 6: (a) Illustration of the change of orientation between two consecutive sections
 594 and (b) Bundle with local twisting



595 **Figure 7: (a) Example of elementary fibre disposition which could induce a change of**
 596 **orientation of the cross-section according to our calculation method, (b) 3D**
 597 **reconstruction of the outer contour of bundle with little morphological variation, c) 3D**
 598 **reconstruction of the outer contour of bundle with strong morphological variations, d) A**
 599 **3D reconstructed bundle with the average values of lengthwise evolution of the cross-**
 600 **section and e) 3D reconstruction of a bundle outer contour by X-ray nanotomography**
 601 **(Del Mastro, 2018)**